BG Pulse Journal USA
ISSN:1947-2536 http://www.bgpulseusa.com/index.php/bg
BG PULSE JOURNAL

POLARIZED ABSORPTION SPECTRA AND MAGNETIC ANISOTROPY OF THE Dy^{3+} ION IN $DyAlO_3$: FROM J-MIXING TO MAGNETO-OPTICAL APPLICATIONS

Usmonova Bakhtiniso Sharif qizi
Lecturer, Department of Exact Sciences,
Bukhara State Technical University,
Bukhara, Uzbekistan
usmonova.baxtinis93@gmail.com
https://doi.org/10.5281/zenodo.23245342

Abstract. Dysprosium orthoaluminate $DyAlO_3$ combines a strongly anisotropic Kramers ion with a low-symmetry (C_s) crystal-field site, which makes it a model system for relating optical selection rules to macroscopic magnetic anisotropy. This study analyses the polarized absorption spectra of the $^6H_{15/2} \rightarrow {}^6F_{3/2}$ band of Dy^{3+} in $DyAlO_3$ at 77 and 300 K together with published magnetic and magneto-optical data. Eight Stark components recorded in two orthogonal polarizations in the ab plane were used to reconstruct the energies of the four lowest Kramers doublets of the ground multiplet (0, 53.7 ± 0.9, 125.7 ± 0.9 and 205.5 ± 0.3 cm^{-1}) and the splitting of the excited $^6F_{3/2}$ multiplet (10.1 ± 1.3 cm^{-1}). Boltzmann analysis shows that 33% of the Dy^{3+} ions occupy excited doublets at 77 K and 63% at 300 K, so the magnetic anisotropy observed above 100 K is controlled by the excited doublets rather than by the ground doublet alone. For a pure $|\pm 15/2\rangle$ ground doublet the model gives $g_{\parallel} = 20$, $g_{\perp} \approx 0$ and a Curie constant along the Ising axis 2.6 times that of the free ion. Judd–Ofelt selection rules show that the $^6H_{15/2} \rightarrow {}^6F_{3/2}$ transition is governed by the Ω_6 parameter alone and that, in the axial approximation, only one of the two $^6F_{3/2}$ sublevels can be reached from a pure $|\pm 15/2\rangle$ state. The observation of both components from the lowest doublet therefore requires J-mixing of the excited states. A two-site geometric model links the sign of the polarization anisotropy to the π or σ character of each transition. Single-oscillator analysis of the Faraday effect (λ_0 = 190 nm, 6.53 eV) indicates that the paramagnetic Verdet constant decreases 3.3-fold between 440 and 750 nm. The results support the use of $DyAlO_3$ in magneto-optical devices and low-temperature magnetic refrigeration.

Keywords: $DyAlO_3$, Dy^{3+}, polarized absorption, Kramers doublets, J-mixing, crystal field, Ising anisotropy, magnetic susceptibility, Faraday effect, Judd–Ofelt theory.

Introduction. Rare-earth orthoaluminates $RAlO_3$ (R is a trivalent rare-earth ion) attract attention in condensed matter physics because the electronic structure of the R^{3+} ion in a low-symmetry crystal field gives them an unusual combination of magnetic and optical properties [1]. Dysprosium orthoaluminate $DyAlO_3$ holds a special place in this family. The Dy^{3+} ion has the $4f^9$ configuration with an odd number of 4f electrons, so by Kramers' theorem every level remains at least doubly degenerate in any electrostatic field and each multiplet splits into Kramers doublets [2, 3].

In the orthoaluminate lattice, Dy^{3+} occupies a site of local symmetry C_s, with a distinguished anisotropy axis lying in the mirror plane of the crystal field [4]. Because the uniaxial component of the crystal field is large, the wave functions of the Kramers doublets of the $^6H_{15/2}$ ground multiplet can be approximated by states $|\pm M_J\rangle$ with large $|M_J|$. Such doublets have a strongly anisotropic g-tensor and are called Ising doublets [5].

Absorption spectroscopy in linearly polarized light gives direct access to the symmetry and composition of these wave functions, because the matrix elements of the electric-dipole operator

depend on the orientation of the light polarization relative to the anisotropy axis [6]. Comparing polarized spectra with magnetic measurements then links the electronic structure of the ion to the macroscopic magnetic behaviour of the crystal [7]. Earlier work established the Ising character of the ground doublet [1, 5], but three questions remain open: how far the Ising behaviour extends into the excited doublets that become populated at elevated temperature, why the polarization anisotropy differs so strongly between Stark components of the same band, and how these microscopic features translate into the magneto-optical response that makes $DyAlO_3$ attractive for applications.

The aim of this work is to establish, quantitatively where possible, the link between the character of the Kramers-doublet wave functions of Dy^{3+} in $DyAlO_3$ and the observed anisotropy of optical absorption, magnetic susceptibility and Faraday rotation. The objectives are:

– to reconstruct the energies of the lowest Kramers doublets of $^6H_{15/2}$ and the splitting of $^6F_{3/2}$ from the polarized Stark components;

– to quantify the thermal population of the doublets between 4.2 and 300 K and its consequences for magnetic anisotropy;

– to derive the Ising g-factors and Curie constants expected for pure $|\pm M_J\rangle$ doublets;

– to analyse the selection rules of the $^6H_{15/2} \rightarrow {}^6F_{3/2}$ transition and the role of J-mixing;

– to evaluate the dispersion of the paramagnetic Faraday effect and assess application prospects.

Materials and methods. Crystal and electronic structure. $DyAlO_3$ crystallizes in an orthorhombic, distorted-perovskite structure (space group Pbnm, or Pnma in the alternative setting) with lattice parameters a ≈ 5.21 Å, b ≈ 5.31 Å and c ≈ 7.40 Å [8]. The Dy^{3+} ion occupies a site of point symmetry C_s (C_{1h}), whose mirror plane coincides with the crystallographic ab plane [4]. There are two magnetically inequivalent Dy sites whose local anisotropy axes lie in the ab plane, symmetric with respect to the crystallographic axes. In the LS-coupling approximation the $4f^9$ configuration gives the $^6H_{15/2}$ ground term. In a field of C_s symmetry, the number of Kramers doublets produced by a multiplet with total angular momentum J is

$$N_D = J + \frac{1}{2}, \quad (1)$$

so that $^6H_{15/2}$ splits into eight doublets, while the excited multiplets $^6F_{3/2}$ and $^6F_{5/2}$ split into two and three doublets, respectively [9]. The crystal-field Hamiltonian for C_s symmetry contains 15 parameters, 14 of which are independent once the orientation of the coordinate frame is fixed [10]. Table 1 summarizes the multiplets relevant to this study.

Table 1. Stark structure of the Dy^{3+} multiplets analysed in this work

Multiplet	J	Kramers doublets, J + 1/2	Approximate energy, cm^{-1}	Role in this study
$^6H_{15/2}$	15/2	8	0–~10^3	ground multiplet; four lowest doublets resolved
$^6F_{5/2}$	5/2	3	≈ 12 400 [11]	nearest neighbour of $^6F_{3/2}$; source of J-mixing
$^6F_{3/2}$	3/2	2	13 088–13 305	final states of the analysed band

Source: compiled by the author; $^6F_{5/2}$ position after free-ion data [11], $^6F_{3/2}$ range from Table 2.

Polarized absorption measurements. Absorption spectra of $DyAlO_3$ single crystals were recorded in linearly polarized light in the region of the $^6H_{15/2} \rightarrow {}^6F_{3/2}$ transition (13 080–13 310 cm^{-1}, 751–765 nm) at 77 and 300 K [1, 12]. The electric vector E of the light wave was oriented along two mutually orthogonal crystallographic axes in the ab plane. The energies of the Stark components were taken from the positions of the absorption maxima.

Magnetic and magneto-optical data. The temperature dependence of the magnetic susceptibility $\chi(T)$ along the three crystallographic axes in the range 78–300 K was taken from [13]; magnetization data in pulsed fields up to 40 T from [4]; Faraday-rotation data in the 440–750 nm range at 90 and 300 K from [5, 6].

Analysis. The energies of the ground doublets K = II, III, IV relative to the lowest doublet I were obtained independently from the two series of transitions ending on the $^6F_{3/2}$ sublevels a and b, and the $^6F_{3/2}$ splitting δ from each ground doublet:

$$\Delta_K = E(I \rightarrow x) - E(K \rightarrow x), \quad x = a,b; \quad \delta_K = E(K \rightarrow b) - E(K \rightarrow a). \tag{2}$$

The relative populations of the doublets were calculated from the Boltzmann distribution over the four resolved doublets:

$$n_i(T) = \frac{\exp(-\Delta_i / k_B T)}{\sum_{j=I}^{IV} \exp(-\Delta_j / k_B T)}, \tag{3}$$

where $k_B = 0.6950\ cm^{-1}/K$. Because the four upper doublets of $^6H_{15/2}$ were not resolved, Eq. (3) overestimates the population of the lowest doublets at room temperature; the values at 300 K should be treated as upper bounds. For a doublet described by pure states $|\pm M_J\rangle$ of a multiplet with Landé factor g_J ($g_J = 4/3$ for $^6H_{15/2}$), the principal g-values are [14]

$$g_{\parallel} = 2 g_J |M_J|, \quad g_{\perp} = 0 \quad (|M_J| > 1/2), \tag{4}$$

and the molar Curie constant (cgs units) is $C = 0.12505 \cdot \mu^2$ emu·K/mol, where μ (in μ_B) equals $\mu_{eff} = g_J[J(J+1)]^{1/2}$ for the free ion and $\sqrt{3} \cdot g_J |M_J|$ along the axis of an Ising doublet:

$$\chi_{\parallel} = \frac{N_A (g_J M_J \mu_B)^2}{k_B T}, \quad \chi_{free} = \frac{N_A g_J^2 \mu_B^2 J(J+1)}{3 k_B T}. \tag{5}$$

Polarization ratios were interpreted with a two-site model. For a transition whose dipole moment is parallel to the local Ising axis (π-type) or perpendicular to it within the ab plane (σ-type), averaging over the two sites with axes at ±φ to the a axis gives

$$R_{\pi} = \frac{I_a}{I_b} = \cot^2 \varphi, \quad R_{\sigma} = \tan^2 \varphi. \tag{6}$$

The intensities of the forced electric-dipole 4f–4f transitions were analysed within Judd–Ofelt theory [15–17], in which the effective dipole operator is

$$D_q^{(eff)} = \sum_{\lambda=2,4,6} \sum_{t,p} (2\lambda+1) A_{tp} \Xi(t,\lambda) (1\ \lambda\ t;\ q, -p-q, p) U_{p+q}^{(\lambda)} \tag{7}$$

where q = 0 corresponds to π and q = ±1 to σ polarization relative to the local axis, A_{tp} are the odd-rank (t = 3, 5, 7) crystal-field parameters, $\Xi(t,\lambda)$ are radial integrals and $U^{(\lambda)}$ are unit tensor operators [15, 17]. Within a single pure J multiplet, the triangle rule $|J - J'| \le \lambda \le J + J'$ and the projection rule $|M' - M| = |p + q| \le \lambda$ apply. J-mixing means that the crystal field admixes states of neighbouring multiplets with different J of the same $4f^9$ configuration into each Stark level [18]. Finally, the dispersion of the paramagnetic Faraday rotation was described in the single-oscillator approximation [5, 6]:

$$V_p(\lambda,T) = C_p(\lambda) \chi(T), \quad C_p(\lambda) \propto \frac{\lambda_0^2}{\lambda^2 - \lambda_0^2}, \tag{8}$$

where $\lambda_0 = 2\pi c/\omega_0$ is the wavelength of the effective allowed transition.

Results. Stark structure of the $^6H_{15/2} \rightarrow {}^6F_{3/2}$ band. The band contains eight Stark components (Table 2). They are labelled by the ground doublet (I–IV) and by the final $^6F_{3/2}$ sublevel (a or b),

and their polarization behaviour is markedly different. Component 2 (transition Ia) has comparable intensity in both polarizations, component 3 (transition IIb) is observed only for E ⊥ b, and the components IIa, IIIa and IVa are strongly anisotropic [1].

Table 2. Stark components of the $^6H_{15/2} \rightarrow {}^6F_{3/2}$ absorption band of Dy^{3+} in $DyAlO_3$

No.	Energy, cm^{-1}	λ, nm	Transition	Polarization behaviour
1	13 304.6	751.6	Ib	not reported
2	13 293.7	752.2	Ia	comparable intensity for both polarizations
3	13 250.0	754.7	IIb	observed only for E ⊥ b
4	13 241.0	755.2	IIa	strongly anisotropic
5	13 178.0	758.8	IIIb	not reported
6	13 169.0	759.4	IIIa	strongly anisotropic
7	13 099.4	763.4	IVb	not reported
8	13 088.0	764.1	IVa	strongly anisotropic

Source: component energies from [12]; polarization behaviour from [1]; wavelengths (in vacuum) calculated by the author.

Applying Eq. (2) to both transition series gives the doublet energies in Table 3. The a and b series agree within 1.9 cm^{-1} for every doublet, which confirms the assignment of the components. The $^6F_{3/2}$ splitting obtained from the four ground doublets is 10.1 ± 1.3 cm^{-1} (mean ± standard deviation), consistent with the earlier estimate of 11 ± 2 cm^{-1} [12]. The value for doublet IV, 205.5 cm^{-1}, lies at the lower edge of the earlier estimate of 208 ± 3 cm^{-1}. The resulting level scheme is shown in Fig. 1.

Table 3. Energies of the lowest Kramers doublets of $^6H_{15/2}$ and splitting of $^6F_{3/2}$

Quantity	From a series, cm^{-1}	From b series, cm^{-1}	Mean, cm^{-1}	Δ/k_B, K	Earlier estimate [12], cm^{-1}
Δ_{II}	52.7	54.6	53.7 ± 0.9	77.2	54 ± 2
Δ_{III}	124.7	126.6	125.7 ± 0.9	180.8	126 ± 2
Δ_{IV}	205.7	205.2	205.5 ± 0.3	295.6	208 ± 3
δ ($^6F_{3/2}$)	10.9; 9.0; 9.0; 11.4 (from I–IV)		10.1 ± 1.3	14.5	11 ± 2

Source: calculated by the author with Eq. (2) from the data of Table 2; uncertainties are half the difference between the two series (Δ) or the standard deviation over four values (δ).

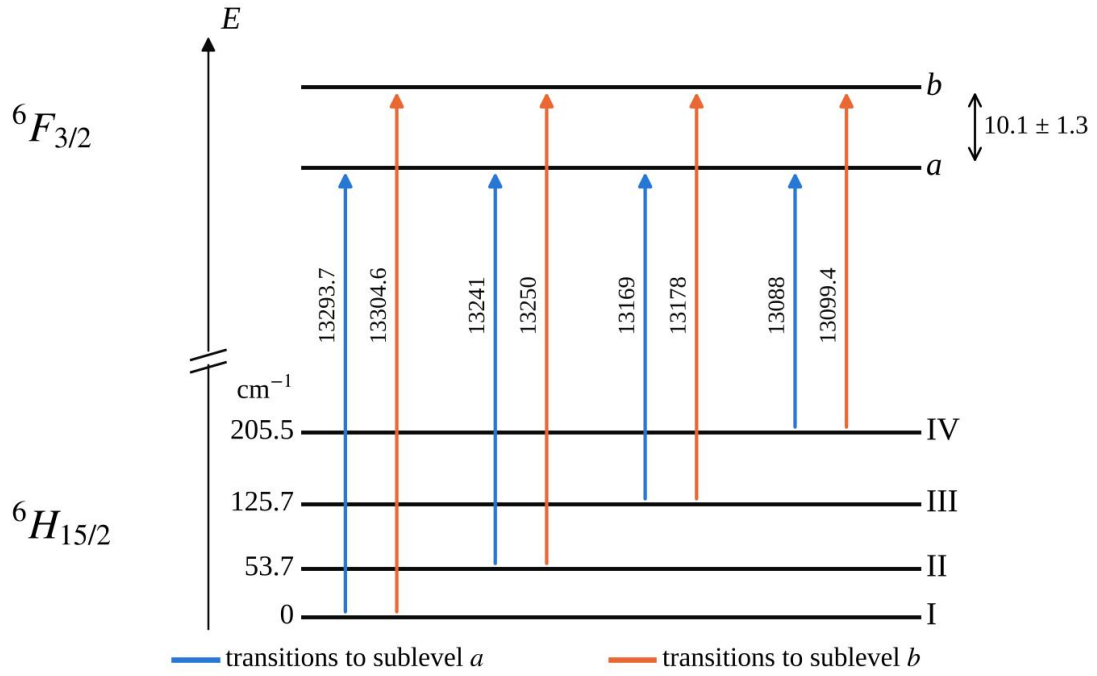


Figure 1. Stark sublevels of the $^6H_{15/2}$ and $^6F_{3/2}$ multiplets of Dy^{3+} in $DyAlO_3$ and the identified transitions (energies in cm^{-1}; the energy axis is broken and not to scale). Constructed by the author from Tables 2 and 3.

Thermal population of the ground-multiplet doublets. The doublet energies fall in the range of thermal energies covered by the experiments: k_BT equals 53.5 cm^{-1} at 77 K, which almost coincides with Δ_{II}, and 208.5 cm^{-1} at 300 K, which almost coincides with Δ_{IV}. The populations calculated with Eq. (3) are listed in Table 4 and plotted in Fig. 2. Below 20 K practically all ions are in the lowest doublet. At 77 K one third of the ions (32.6%) already occupy doublets II–IV, and above about 150 K the excited doublets together hold more than half of the population.

Table 4. Relative populations (%) of the four lowest Kramers doublets of $^6H_{15/2}$

T, K	I	II	III	IV	Outside doublet I
4.2	100.0	0.0	0.0	0.0	0.0
20	97.9	2.1	0.0	0.0	2.1
77	67.4	24.7	6.4	1.4	32.6
150	49.1	29.3	14.7	6.8	50.9
300	37.1	28.7	20.3	13.9	62.9

Source: calculated by the author with Eq. (3); the unresolved upper doublets V–VIII are neglected, so the 300 K values for doublet I are upper bounds.

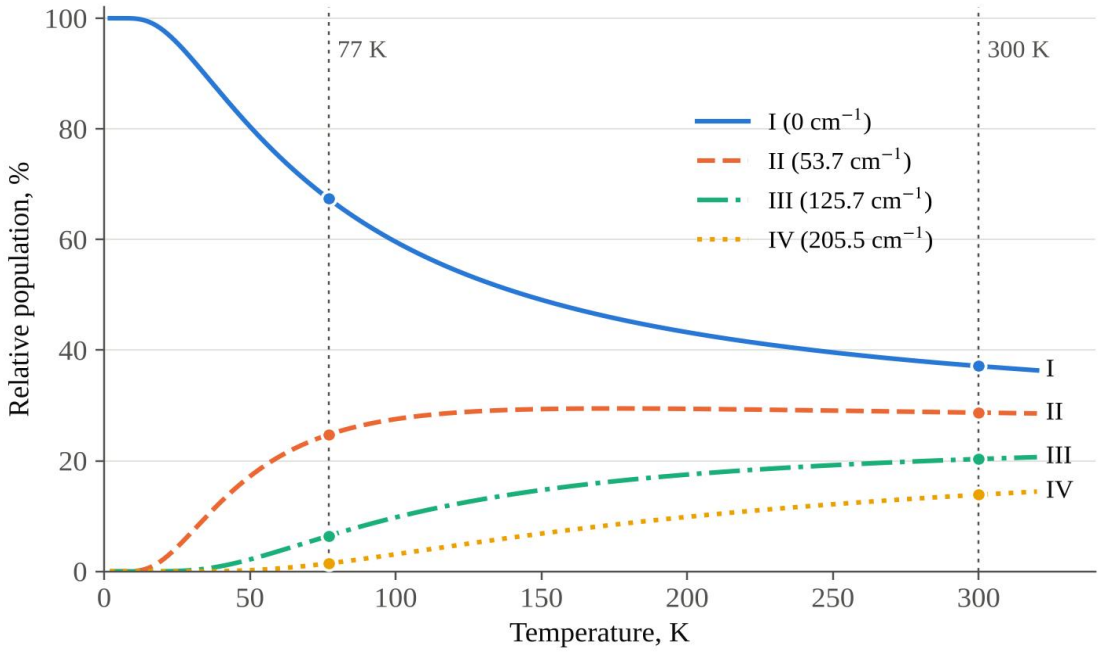


Figure 2. Temperature dependence of the relative populations of the Kramers doublets I–IV of the $^6H_{15/2}$ multiplet; markers show the measurement temperatures 77 and 300 K. Calculated by the author.

Ising parameters and magnetic anisotropy. Table 5 lists the g-values that Eq. (4) predicts for pure $|\pm M_J\rangle$ doublets of $^6H_{15/2}$. All doublets with $|M_J| \geq 3/2$ are Ising-like ($g_\perp = 0$), and their longitudinal g-factors decrease linearly from 20 for $|\pm 15/2\rangle$ to 4 for $|\pm 3/2\rangle$. Only the $|\pm 1/2\rangle$ doublet is strongly non-Ising, with $g_\perp = 10.67$ exceeding $g_{//}$. This point matters for interpretation: the Ising character requires large $|M_J|$, and doublets close to $|\pm 1/2\rangle$ cannot produce Ising behaviour.

Table 5. Principal g-values and magnetic moments of pure $|\pm M_J\rangle$ doublets of the $^6H_{15/2}$ multiplet ($g_J = 4/3$)

$\|M_J\|$	$g_{//}$	$g_\perp$	$\mu_{//} = g_J\|M_J\|, \mu_B$	Character
15/2	20.00	0	10.00	Ising
13/2	17.33	0	8.67	Ising
11/2	14.67	0	7.33	Ising
9/2	12.00	0	6.00	Ising
7/2	9.33	0	4.67	Ising
5/2	6.67	0	3.33	Ising
3/2	4.00	0	2.00	Ising
1/2	1.33	10.67	0.67	easy-plane (non-Ising)

Source: calculated by the author with Eq. (4).

Table 6 compares the Curie constants of the free ion and of an Ising $|\pm 15/2\rangle$ doublet obtained from Eq. (5). Along the Ising axis, the Curie constant is 2.65 times that of the free ion, while the Curie contribution perpendicular to the axis vanishes and the transverse susceptibility is limited to

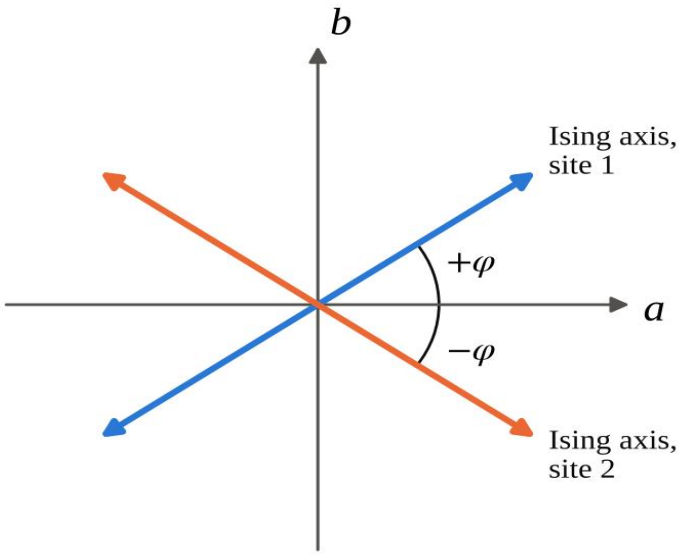
the temperature-independent van Vleck term. The orientational average of the Ising doublet (12.5 emu·K/mol) lies 12% below the free-ion value, so measurements on powders alone cannot reveal the Ising character, whereas single-crystal measurements along different axes reveal it directly.

Table 6. Molar Curie constants of Dy^{3+} for the free ion and for an Ising $|\pm 15/2\rangle$ ground doublet

Case	μ^2, μ_B^2	C, emu·K/mol	Ratio to free ion
Free ion, isotropic ($\mu_{eff} = 10.65\ \mu_B$)	113.3	14.17	1.00
Ising doublet, field along the Ising axis	300.0	37.52	2.65
Ising doublet, field perpendicular to the axis	0	≈ 0 (van Vleck term only)	≈ 0
Ising doublet, orientational average	100.0	12.51	0.88

Source: calculated by the author with Eq. (5); $C = 0.12505 \cdot \mu^2$ emu·K/mol.

Polarization analysis. Figure 3 shows the geometry behind Eq. (6). Because the Ising axes of the two inequivalent sites lie at ±φ to the a axis, light polarized along a or b projects onto both of them with the same weight, and the polarization ratio identifies the character of a transition. A π-type transition gives $I_a/I_b = \cot^2\varphi$, and a σ-type transition gives the inverse ratio, $\tan^2\varphi$. Components that are strong for E ∥ a and weak for E ∥ b (or vice versa) therefore have a dominant π or σ character, depending on whether φ is smaller or larger than 45°. Component IIb, observed only for E ⊥ b, is close to the pure limit. A ratio close to unity, as observed for component Ia, can arise in this model only if φ ≈ 45° or if the transition has mixed π/σ character. The first possibility is excluded by the strong anisotropy of the other components measured on the same crystal, so the transition Ia must have mixed polarization character.



$E \parallel a$: π-type $\propto \cos^2\varphi$, σ-type $\propto \sin^2\varphi$
$E \parallel b$: π-type $\propto \sin^2\varphi$, σ-type $\propto \cos^2\varphi$

Figure 3. Orientation of the local Ising axes of the two magnetically inequivalent Dy^{3+} sites in the ab plane and the resulting polarization weights of π- and σ-type transitions (schematic; the angle φ is not to scale). Drawn by the author.

Magneto-optical parameters. Faraday-rotation measurements on $DyAlO_3$ at 90 and 300 K showed a linear dependence of the Verdet constant V on the magnetic susceptibility χ at 506 nm, which gives a paramagnetic Verdet constant $C_p = (6.51 \pm 0.3)\times10^3$ min/(cm·Oe) [5, 6]. This value is several times larger than for dysprosium aluminium garnet $Dy_3Al_5O_{12}$; the difference is attributed to the effect of the low-symmetry orthorhombic crystal field on the excited $4f^85d$ states of the magneto-active ion [5]. The effective frequency of the allowed transitions, $\omega_0 = 9.9\times10^{15}$ s^{-1}, corresponds to $\lambda_0 = 190$ nm, a photon energy of 6.53 eV and a wavenumber of 52 600 cm^{-1} (Table 7). This places the effective transition in the 4f → 5d region, four times higher in energy than the 4f–4f band analysed above.

Table 7. Magneto-optical parameters of Dy^{3+} in $DyAlO_3$

Parameter	Value	Source
Paramagnetic Verdet constant C_p (506 nm)	$(6.51 \pm 0.3)\times10^3$ min/(cm·Oe)	[5, 6]
Effective frequency ω_0	9.9×10^{15} s^{-1}	[5]
Effective wavelength $\lambda_0 = 2\pi c/\omega_0$	190 nm	calculated
Photon energy $\hbar\omega_0$	6.53 eV	calculated
Wavenumber $1/\lambda_0$	52 600 cm^{-1}	calculated
V_p(440 nm)/V_p(506 nm)	1.40	calculated, Eq. (8)
V_p(750 nm)/V_p(506 nm)	0.42	calculated, Eq. (8)

Source: compiled and calculated by the author.

The dispersion predicted by Eq. (8) with λ_0 = 190 nm is shown in Fig. 4. Across the measured range the normalized paramagnetic Verdet constant falls from 1.40 at 440 nm to 0.42 at 750 nm, i.e. by a factor of 3.3. The $^6H_{15/2} \rightarrow {}^6F_{3/2}$ band at 752–764 nm lies just beyond the long-wavelength end of this range, where resonant 4f–4f contributions are expected to perturb the single-oscillator dispersion.

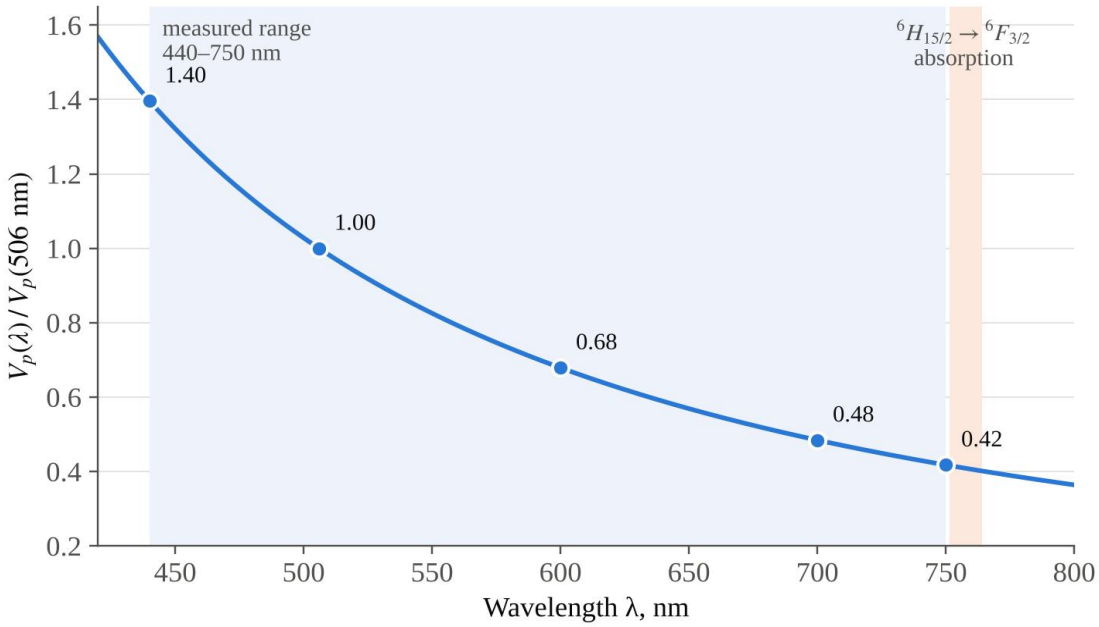


Figure 4. Dispersion of the paramagnetic Verdet constant of $DyAlO_3$ in the single-oscillator approximation (λ_0 = 190 nm), normalized to 506 nm. The shaded areas mark the measured range and the $^6H_{15/2} \rightarrow {}^6F_{3/2}$ absorption band. Calculated by the author.

Discussion. J-mixing as the origin of the anomalous polarization. The selection rules make the role of J-mixing explicit. For $^6H_{15/2} \rightarrow {}^6F_{3/2}$, $|J - J'| = 6$, so the triangle rule leaves only the $\lambda = 6$ term of Eq. (7). The transition is therefore governed by the Judd–Ofelt parameter Ω_6 alone [15, 16]. In the axial approximation, the two Kramers sublevels of $^6F_{3/2}$ are close to $|\pm 1/2\rangle$ and $|\pm 3/2\rangle$. Starting from a pure $|\pm 15/2\rangle$ ground doublet, the projection rule $|\Delta M| \leq 6$ allows a transition only to the $|\pm 3/2\rangle$ sublevel ($|\Delta M| = 6$); reaching $|\pm 1/2\rangle$ would require $|\Delta M| = 7$. In the pure-state limit, only one of the components Ia and Ib should therefore be observed. Both are in fact observed, and component Ia additionally shows nearly isotropic polarization. This can be explained if the $^6F_{3/2}$ sublevels contain admixtures of other J states, primarily of $^6F_{5/2}$ ($|M'| = 5/2$), which lies only about 800 cm^{-1} below [11]. Such admixtures relax both the triangle and the projection restrictions [17, 18]. This analysis supports the conclusion that intra-multiplet mixing alone cannot account for the spectra and that J-mixing must be included [1, 18]. The relative intensity of the nominally forbidden component of the Ia/Ib pair provides a direct, measurable index of the degree of J-mixing.

For the upper doublets, which are not pure $|\pm 15/2\rangle$ states, transitions to both $^6F_{3/2}$ sublevels are allowed by the projection rule; for a $|\pm 13/2\rangle$ doublet, for example, $|\Delta M| = 5$ and 6. The appearance of all eight components (Table 2) is therefore consistent with the expected selection rules, and the information is carried mainly by their polarization ratios. The two-site model (Eq. (6), Fig. 3) turns these ratios into a classification of π- and σ-type transitions. Once the angle φ is

determined independently, for example from neutron diffraction or from the angular dependence of the magnetization, the measured ratios will give the weights of $|M_J\rangle$ components in each doublet.

Ising character beyond the ground doublet. The thermal analysis shows why the magnetic anisotropy of $DyAlO_3$ persists at $T \geq 100$ K [7, 13]. At 100 K, 40% of the ions are in doublets II–IV, and above about 150 K these doublets hold most of the population (Table 4). If these doublets were close to $|\pm 1/2\rangle$, the high-temperature susceptibility would become nearly isotropic, since a $|\pm 1/2\rangle$ doublet has $g_\perp > g_{//}$ (Table 5). The persistence of strong anisotropy therefore implies that doublets II–IV also have predominantly large $|M_J|$ components, i.e. Ising-like character. This agrees with the conclusion that Ising behaviour extends over a significant part of the energy spectrum of the ion [13], with the crystal-field analysis of the van Vleck susceptibility along the c axis [10] and with neutron data indicating strong uniaxial anisotropy of the Dy^{3+} moments [10]. The Curie constants in Table 6 offer a quantitative test: in the low-temperature limit, the single-crystal susceptibility along the Ising direction should approach $C_{//} \approx 37.5$ emu·K/mol (projected onto the measurement axis), and the gradual decrease of the anisotropy with temperature should follow the population curves in Fig. 2.

Magneto-optical and magnetocaloric prospects. The large paramagnetic Verdet constant follows from the same physics: the Faraday rotation of a paramagnetic ion scales with its susceptibility, and the Ising doublet maximizes the susceptibility along the easy direction. In addition, the low-symmetry field enhances the mixing of $4f^8 5d$ states [5, 6]. The 3.3-fold decrease of V_p between 440 and 750 nm (Fig. 4) indicates that blue–green operation gives the strongest rotation, but absorption by the 4f–4f bands must be taken into account when selecting the operating wavelength. Calculations of the magnetic entropy response suggest that, owing to the Ising character of the Dy^{3+} moments, $DyAlO_3$ can be a more efficient magnetic refrigerant in the 4.2–20 K range than the conventional $Dy_3Al_5O_{12}$ [7, 13]. This is consistent with Table 4: below 20 K only the ground doublet is populated, so the full doublet entropy R ln 2 per mole of Dy is available for magnetic cooling. The metamagnetic transitions observed in pulsed fields up to 40 T, which arise from the competition between exchange and crystal-field interactions [4, 8], further widen the range of possible applications.

Limitations. Only four of the eight doublets of $^6H_{15/2}$ were resolved, so the partition function is truncated and the populations at 300 K are upper bounds. Polarization ratios were reported qualitatively; quantitative intensity ratios and the angle φ are needed to extract the composition of the wave functions. The Faraday dispersion is described by a single effective oscillator, which neglects resonant 4f–4f contributions near the absorption bands. Extending the measurements to the $^6H_{15/2} \rightarrow {}^6F_{5/2}$ band and to intermediate temperatures, and fitting the 15 crystal-field parameters jointly to optical and magnetic data, are the next steps.

Conclusion. The analysis of the polarized absorption spectra and magnetic anisotropy of Dy^{3+} in $DyAlO_3$ leads to the following conclusions:

1. The eight Stark components of the $^6H_{15/2} \rightarrow {}^6F_{3/2}$ band yield the energies of the four lowest ground doublets, 0, 53.7 ± 0.9, 125.7 ± 0.9 and 205.5 ± 0.3 cm^{-1}, and a $^6F_{3/2}$ splitting of 10.1 ± 1.3 cm^{-1}; two independent transition series agree within 1.9 cm^{-1}.

2. The excited doublets are thermally significant: 33% of the ions occupy them at 77 K and 63% at 300 K. The magnetic anisotropy observed above 100 K therefore reflects the Ising-like character of these doublets, not only that of the ground doublet.

3. A pure $|\pm 15/2\rangle$ ground doublet gives $g_{\parallel} = 20$, $g_{\perp} = 0$ and a Curie constant along the Ising axis 2.65 times that of the free ion; Ising behaviour requires $|M_J| \geq 3/2$, while a $|\pm 1/2\rangle$ doublet would be easy-plane.

4. The $^6H_{15/2} \rightarrow {}^6F_{3/2}$ transition is governed by Ω_6 alone, and from a pure $|\pm 15/2\rangle$ state only one $^6F_{3/2}$ sublevel is accessible. The observation of both Ia and Ib, with nearly isotropic Ia, demonstrates J-mixing, mainly with $^6F_{5/2}$.

5. In the single-oscillator approximation (λ_0 = 190 nm, 6.53 eV), the paramagnetic Verdet constant decreases 3.3-fold from 440 to 750 nm. Together with the Ising character of Dy^{3+}, this supports the use of $DyAlO_3$ in magneto-optical devices and low-temperature magnetic refrigeration.

The proposed two-site polarization model and the Ia/Ib intensity ratio provide measurable criteria for quantifying J-mixing and the composition of the Kramers-doublet wave functions in rare-earth orthoaluminates.

REFERENCES

1. Faiziev Sh.Sh., Saidov K.S., Nizomova Sh.K. Electronic structure of the ground multiplet of the dysprosium ion in orthoaluminate. Bukhara State University.
2. Gruber J.B., Zandi B., Valiev U.V., Rakhimov Sh.A. Energy levels of $Dy^{3+}(4f^9)$ in orthoaluminate crystals // Journal of Applied Physics. 2003. Vol. 93, No. 2. P. 1030–1034.
3. Kramers H.A. Théorie générale de la rotation paramagnétique dans les cristaux // Proceedings of the Royal Netherlands Academy of Arts and Sciences. 1930. Vol. 33. P. 959–972.
4. Kolmakova N.P., Krynetskii I.B., Lukina M.M., et al. Crystal field and metamagnetic behavior of rare-earth orthoaluminates: $DyAlO_3$ // Physica Status Solidi (b). 1990. Vol. 159, No. 2. P. 465–474. DOI: 10.1002/pssb.2221590217.
5. Valiev U.V., Malysheva M.E., Pelenovich V.O., et al. Magneto-optics of Dy^{3+} ion in low-symmetric orthoaluminate structure // Crystallography Reports. 2023. Vol. 68. P. 1180–1189. DOI: 10.1134/S1063774523060179.
6. Valiev U.V., Malysheva M.E., Vildanov R.R., Turotov F.K. Contribution of 4f→5d transitions to the magneto-optics of the Dy^{3+} ion in the orthoaluminate structure // Uzbek Journal of Physics. 2024. Vol. 26, No. 2.
7. Sultonov O.Z. Specific features of the Faraday effect in rare-earth orthoaluminate $DyAlO_3$ // Optics and Spectroscopy. 2024. Vol. 132, No. 3. P. 245–251.
8. Bidaux R., Bouree J.E., Hammann J. Magnetic properties of $DyAlO_3$ // Journal of Physics and Chemistry of Solids. 1975. Vol. 36, No. 7–8. P. 655–662.
9. Valiev U.V., Saidov K.S., Rakhimov Sh.A. Optical spectra and crystal field of Dy^{3+} in $DyAlO_3$ // Journal of Luminescence. 2000. Vol. 87–89. P. 1063–1065.
10. Amoretti G., Bucci C., Caciuffo R., et al. Crystal field parameters of $DyAlO_3$ from neutron spectroscopy // Journal of Magnetism and Magnetic Materials. 1985. Vol. 49, No. 1–2. P. 53–60.
11. Carnall W.T., Fields P.R., Rajnak K. Electronic energy levels in the trivalent lanthanide aquo ions. I. Pr^{3+}, Nd^{3+}, Pm^{3+}, Sm^{3+}, Dy^{3+}, Ho^{3+}, Er^{3+}, and Tm^{3+} // Journal of Chemical Physics. 1968. Vol. 49, No. 10. P. 4424–4442. DOI: 10.1063/1.1669893.
12. Kolmakova N.P., Levitin R.Z., Popov A.I., et al. Crystal field and magnetic properties of $DyAlO_3$ // Journal of Magnetism and Magnetic Materials. 1989. Vol. 81, No. 1–2. P. 196–200.

13. Abragam A., Bleaney B. Electron Paramagnetic Resonance of Transition Ions. Oxford: Clarendon Press, 1970. 911 p.
14. Judd B.R. Optical absorption intensities of rare-earth ions // Physical Review. 1962. Vol. 127, No. 3. P. 750–761. DOI: 10.1103/PhysRev.127.750.
15. Ofelt G.S. Intensities of crystal spectra of rare-earth ions // Journal of Chemical Physics. 1962. Vol. 37, No. 3. P. 511–520. DOI: 10.1063/1.1701366.
16. Reid M.F., Richardson F.S. Electric dipole intensity parameters for lanthanide 4f–4f transitions // Journal of Chemical Physics. 1983. Vol. 79, No. 12. P. 5735–5745.
17. Downer M.C., Bivas A. J-mixing effects in rare-earth optical spectra // Physical Review B. 1983. Vol. 28, No. 11. P. 6489–6499.